Finite Element Solution of the 3D Compressible Navier–Stokes Equations by a Velocity–Vorticity Method

G. GUEVREMONT, W. G. HABASHI, AND P. L. KOTIUGA

Concordia University, Montreal, Canada H3G 1M8

AND

M. M. HAFEZ

University of California, Davis, California 95616

This paper presents an alternative formulation to the primitive variable form of the Navier–Stokes equations. The approach is based on the use of the velocity and vorticity variables as a logical extension of the stream function–vorticity method which is quite effective for two-dimensional flows. Second-order equations are obtained for the variables and discretization is through a weak-Galerkin finite element method, followed by Newton linearization. The velocity and vorticity components are solved simultaneously by a direct solver. The scheme is demonstrated for two-dimensional and three-dimensional incompressible and subsonic internal enclosed flow problems. © 1993 Academic Press, Inc.

I. INTRODUCTION

The numerical simulation of incompressible and compressible viscous flows remains an area of high activity. The demand for efficient viscous flow methods for the analysis and design of aerodynamic components is growing at an unprecedented pace. Finite difference, finite volume and finite element methods are continuously being developed to respond to these needs.

There is no doubt that primitive variables formulations of the Navier–Stokes equations enjoy a high prominence for solving these equations, especially for three-dimensional problems. For two-dimensional and axisymmetric problems other alternatives exist, such as the stream function–vorticity approach which eliminates pressure as a variable and, in addition, conserves mass identically. Starting with the work of Campion–Renson and Crochet [1], several authors [2–4] have refined the application of the finite element method to the stream function–vorticity approach to the point where, for incompressible high Reynolds and Rayleigh number flows, in complex geometries, artificial viscosity and wall vorticity formulae are completely dispensed with. These approaches are invariably embedded in

a Newton linearization and a direct solver, yielding very stable and fast convergence. The stream function–vorticity method has also been extended to multiple connected domains [5], subsonic [6], transonic [7], and unsteady flows [8].

The extension of such alternative formulations to primitive variables, for 3D flows, has been made but is, to a large degree, not simple. For example, a vector potential [9–11], or a two, and sometimes three, stream functions approach is used to represent arbitrary three-dimensional flows [12–16]. The imposition of the boundary conditions, especially for internal flows, is quite complicated.

A logical extension of the stream function–vorticity approach could, however, be done through the velocity–vorticity formulation, initially suggested by Fasel [17] for two-dimensional flows and by Cook [18] and Dennis, Ingham, and Cook [19] for three-dimensional Navier–Stokes equations. Efforts in that direction have increased and incompressible velocity–vorticity approaches, using finite difference and finite element schemes, have been proposed [20–27]. Compressible flow approaches, by a finite element method, have also been developed in Refs. [26, 27] for two-dimensional cases.

II. THEORETICAL FORMULATION

Governing Equations

The governing equations for three-dimensional, steady, compressible subsonic viscous flow, in terms of the primitive variables (V, p, ρ), are

Continuity,

$$\nabla \cdot (\rho V) = 0; \tag{1}$$

Momentum,

$$\rho(\mathbf{V} \cdot \nabla)\mathbf{V} + \mathbf{V}(\nabla \cdot \rho \mathbf{V})$$

$$= -\nabla p + \frac{1}{\text{Re}}\left[-\frac{2}{3}\nabla(\mu\nabla \cdot \mathbf{V}) \right.$$

$$\left. + \nabla \times \mu(\nabla \times \mathbf{V}) + 2(\nabla \cdot \mu\nabla)\mathbf{V} \right], \qquad (2)$$

where Re is the Reynolds number. These equations are complemented by the energy equation and the equation of state.

Using the vorticity definition and the continuity equation, a second-order form of the velocity–vorticity equations, appropriate for a finite element formulation, can be obtained. For the velocity equations we have

$$\nabla \times \rho\mathbf{\Omega} = \nabla \times (\rho\mathbf{V} \times \mathbf{V}) = \nabla \times [\nabla \times (\rho\mathbf{V}) - \nabla\rho \times \mathbf{V}]$$

$$= \nabla[\nabla \cdot (\rho\mathbf{V})] - \nabla^2(\rho\mathbf{V}) - \nabla \times (\nabla\rho \times \mathbf{V})$$

$$= -\nabla^2(\rho\mathbf{V}) - \nabla \times (\nabla\rho \times \mathbf{V})$$

or

$$\nabla^2(\rho\mathbf{V}) + \nabla \times \rho\mathbf{\Omega} + \nabla \times (\nabla\rho \times \mathbf{V}) = 0. \qquad (3)$$

The vorticity transport equation can be derived by taking the curl of the momentum equations, hence eliminating the pressure as a variable, obtaining

$$\nabla^2(\mu\mathbf{\Omega}) - \text{Re}[(\rho\mathbf{V} \cdot \nabla)\mathbf{\Omega} - (\mathbf{\Omega} \cdot \nabla)\rho\mathbf{V} + \mathbf{S}^\rho] + \mathbf{S}^\mu = 0, \qquad (4)$$

where

$$\mathbf{S}^\rho = \tfrac{1}{2}\nabla\rho \times (\nabla V^2)$$

$$\mathbf{S}^\mu = 2(\nabla \times \mu\nabla^2\mathbf{V} + \nabla \times (\nabla\mu \cdot \nabla)\mathbf{V} - \nabla^2(\mu\mathbf{\Omega})) + \nabla(\mathbf{\Omega} \cdot \nabla\mu)$$

$$= \mathbf{S}_x^{\mu 1} + \mathbf{S}_y^{\mu 2} + \mathbf{S}_z^{\mu 3} \qquad \text{in Cartesian coordinates.}$$

Weak-Galerkin Form

The weighted residual form is obtained by minimizing the residuals of the system of equations over the solution domain. Each equation is multiplied by a weight function, W_i, and integrated over the domain as follows:

$$\int_V W_i^{\mathbf{V}}[\nabla^2(\rho\mathbf{V}) + \nabla \times \rho\mathbf{\Omega} + \nabla \times (\nabla\rho \times \mathbf{V})]\, dV = 0 \qquad (5)$$

$$\int_V W_i^{\mathbf{\Omega}}[\nabla^2(\mu\mathbf{\Omega}) - \text{Re}\{(\rho\mathbf{V} \cdot \nabla)\mathbf{\Omega}$$

$$- (\mathbf{\Omega} \cdot \nabla)\rho\mathbf{V} + \mathbf{S}^\rho\} + \mathbf{S}^\mu]\, dV = 0. \qquad (6)$$

The weak form of these equations is obtained after integration by parts of second-order terms:

$$\int_V [\nabla W_i^{\mathbf{V}} \cdot \nabla(\rho\mathbf{V}) - W_i^{\mathbf{V}}(\nabla \times \rho\mathbf{\Omega}) + \nabla W_i^{\mathbf{V}} \times (\nabla\rho \times \mathbf{V})]\, dV$$

$$- \oint_S W_i^{\mathbf{V}}[\mathbf{n} \cdot \nabla(\rho\mathbf{V}) + \mathbf{n} \times (\nabla\rho \times \mathbf{V})]\, dS = 0 \qquad (7)$$

$$\int_V [\nabla W_i^{\mathbf{\Omega}} \cdot \nabla(\mu\mathbf{\Omega}) + W_i^{\mathbf{\Omega}}\, \text{Re}\{(\rho\mathbf{V} \cdot \nabla)\mathbf{\Omega}$$

$$- (\mathbf{\Omega} \cdot \nabla)\rho\mathbf{V} + \mathbf{S}^\rho\} + W_{ix}^{\mathbf{\Omega}}S^{\mu 1} + W_{iy}^{\mathbf{\Omega}}S^{\mu 2} + W_{iz}^{\mathbf{\Omega}}S^{\mu 3}]\, dV$$

$$- \oint_S W_i^{\mathbf{\Omega}}[n \cdot \nabla(\mu\mathbf{\Omega}) + S^{\mu 1}\, dy\, dz$$

$$+ S^{\mu 2}\, dz\, dx + S^{\mu 3}\, dx\, dy] = 0. \qquad (8)$$

Newton Linearization

The nonlinear system of Eqs. (7), (8) is linearized by a Newton method. All three velocity components with all three vorticity components are solved simultaneously. Each vector is expressed in Δ form as

$$\Delta\mathbf{V} = \mathbf{V}^{n+1} - \mathbf{V}^n \qquad (9)$$

$$\Delta\mathbf{\Omega} = \mathbf{\Omega}^{n+1} - \mathbf{\Omega}^n. \qquad (10)$$

Upon substitution in Eqs. (7), (8) and retaining only first-order terms, the system of equations can be re-expressed as

$$\int_V [\nabla W_i^{\mathbf{V}} \cdot \nabla(\rho\,\Delta\mathbf{V}) - W_i^{\mathbf{V}}(\nabla \times \rho\,\Delta\mathbf{\Omega})$$

$$+ \nabla W_i^{\mathbf{V}} \times (\nabla\rho \times \Delta\mathbf{V})]\, dV = -(R)_{\mathbf{V}_i} \qquad (11)$$

$$\int_V [\nabla W_i^{\mathbf{\Omega}} \cdot \nabla(\mu\,\Delta\mathbf{\Omega}) + W_i^{\mathbf{\Omega}}\, \text{Re}\{(\rho\mathbf{V} \cdot \nabla)\,\Delta\mathbf{\Omega}$$

$$+ (\rho\,\Delta\mathbf{V} \cdot \nabla)\mathbf{\Omega} - (\mathbf{\Omega} \cdot \nabla)\rho\,\Delta\mathbf{V} - (\Delta\mathbf{\Omega} \cdot \nabla)\rho\mathbf{V} + \Delta\mathbf{S}^\rho\}$$

$$+ W_{ix}^{\mathbf{\Omega}}\,\Delta S^{\mu 1} + W_{iy}^{\mathbf{\Omega}}\,\Delta S^{\mu 2} + W_{iz}^{\mathbf{\Omega}}\,\Delta S^{\mu 3}]\, dV = -(R)_{\mathbf{\Omega}_i}, \qquad (12)$$

where

$$\Delta\mathbf{S}^\rho = \nabla\rho \times \nabla(\mathbf{V} \cdot \Delta\mathbf{V})$$

$$\Delta\mathbf{S}^\mu = 2\{\nabla \times \mu\nabla^2\,\Delta\mathbf{V} + \nabla \times (\nabla\mu \cdot \nabla)\,\Delta\mathbf{V}$$

$$- \nabla^2\mu\,\Delta\mathbf{\Omega}\} + \nabla(\nabla\mu \cdot \Delta\mathbf{\Omega})$$

$$= \Delta\mathbf{S}_x^{\mu 1} + \Delta\mathbf{S}_y^{\mu 2} + \Delta\mathbf{S}_z^{\mu 3}$$

and R_i's are the residuals, at node i, of the discretized governing equations.

Finite Element Discretization

The geometry discretization is based on curvilinear isoparametric twenty node elements. For equal degrees of approximation of vorticity and derivatives of velocity, the former is represented by trilinear shape functions, while the velocity is approximated by triquadratic shape functions. Hence for the velocity vector,

$$V = \sum_{j=1}^{20} N_j^V V_j \qquad (13)$$

while for the vorticity vector,

$$\Omega = \sum_{j=1}^{8} N_j^\Omega \Omega_j. \qquad (14)$$

The weight functions, W_i, in the Galerkin finite element scheme are chosen to be the corresponding shape functions. Substituting and assembling over the elements, one obtains the set of discretized equations for the velocity vector,

$$\sum_{e=1}^{E} \left[\sum_{j=1}^{20} [k_{VV}]_{ij} \Delta V_j + \sum_{j=1}^{8} [k_{V\Omega}]_{ij} \Delta \Omega_j \right] = -(R)_{V_i}, \qquad (15)$$

where, for example, for the w-velocity component,

$$[k_{i,j}^u]_w = \int_V N_{i,x}^V \rho_z N_j^V \, dV$$

$$[k_{i,j}^v]_w = \int_V N_{i,y}^V \rho_z N_j^V \, dV$$

$$[k_{i,j}^w]_w = \int_V [\rho(N_{i,x}^V N_{j,x}^V + N_{i,y}^V N_{j,y}^V + N_{i,z}^V N_{j,z}^V) + N_{i,z}^V \rho_z N_j^V] \, dV$$

$$[k_{i,j}^{\Omega_1}]_w = \int (N_i^V \rho N_{j,y}^\Omega + N_i^V \rho_y N_j^\Omega) \, dV$$

$$[k_{i,j}^{\Omega_2}]_w = -\int_V (N_i^V \rho N_{j,x}^\Omega + N_i^V \rho_x N_j^\Omega) \, dV$$

$$[k_{i,j}^{\Omega_3}]_w = 0.$$

The following set of discretized equations is obtained for the vorticity vector

$$\sum_{e=1}^{E} \left[\sum_{j=1}^{8} [k_{\Omega\Omega}]_{ij} \Delta \Omega_j + \sum_{j=1}^{20} [k_{\Omega V}]_{ij} \Delta V_j \right] = -(R)_{\Omega_i}, \qquad (16)$$

where, for example, for the Ω_1-vorticity component,

$$[k_{i,j}^u]_{\Omega_1} = \int_V [N_i^\Omega \operatorname{Re}(\rho \Omega_{1,x} N_j^V - \rho \Omega_1 N_{j,x}^V$$
$$- \rho_x \Omega_1 N_j^V - \rho \Omega_2 N_{j,y}^V - \rho_y \Omega_2 N_j^V - \rho \Omega_3 N_{j,z}^V$$
$$- \rho_z \Omega_3 N_j^V + \rho_y u N_{j,z}^V + \rho_y u_z N_j^V$$
$$- \rho_z u N_{j,y}^V - \rho_z u_y N_j^V)$$
$$+ 2N_{i,x}^\Omega (\mu_y N_{j,z}^V - \mu_z N_{j,y}^V)] \, dV$$

$$[k_{i,j}^v]_{\Omega_1} = \int_V [N_i^\Omega \operatorname{Re}(\rho \Omega_{1,y} N_j^V + \rho_y v N_{j,z}^V$$
$$+ \rho_y v_z N_j^V - \rho_z v N_{j,y}^V - \rho_z v_y N_j^V)$$
$$+ 2N_{i,y}^\Omega (\mu_y N_{j,z}^V - \mu_z N_{j,y}^V)] \, dV$$

$$[k_{i,j}^w]_{\Omega_1} = \int_V [N_i^\Omega \operatorname{Re}(\rho \Omega_{1,z} N_j^V + \rho_y w N_{j,z}^V$$
$$+ \rho_y w_z N_j^V - \rho_z w N_{j,y}^V - \rho_z w_y N_j^V)$$
$$+ 2N_{i,z}^\Omega (\mu_y N_{j,z}^V - \mu_z N_{j,y}^V)] \, dV$$

$$[k_{i,j}^{\Omega_1}]_{\Omega_1} = \int_V [N_{i,x}^\Omega \mu N_{j,x}^\Omega + N_{i,y}^\Omega (\mu N_{j,y}^\Omega + \mu_y N_j^\Omega)$$
$$+ N_{i,z}^\Omega (\mu N_{j,z}^\Omega + \mu_z N_j^\Omega)$$
$$+ N_i^\Omega \operatorname{Re}(\rho u N_{j,x}^\Omega + \rho v N_{j,y}^\Omega + \rho w N_{j,z}^\Omega$$
$$- \rho_x u N_j^\Omega - \rho u_x N_j^\Omega)] \, dV$$

$$[k_{i,j}^{\Omega_2}]_{\Omega_1} = -\int_V [N_i^\Omega \operatorname{Re}(\rho_y u N_j^\Omega + \rho u_y N_j^\Omega)$$
$$+ N_{i,x}^\Omega \mu_y N_j^\Omega] \, dV$$

$$[k_{i,j}^{\Omega_3}]_{\Omega_1} = -\int_V [N_i^\Omega \operatorname{Re}(\rho_z u N_j^\Omega + \rho u_z N_j^\Omega)$$
$$+ N_{i,x}^\Omega \mu_z N_j^\Omega] \, dV.$$

III. BOUNDARY CONDITIONS

Inlet and Exit Boundary Conditions

For through-flow type problems, the velocity distribution is specified at inlet and the vorticity is therefore known:

$$V = V(y, z) \qquad (17)$$

$$\Omega = \Omega(y, z). \qquad (18)$$

In the derivation of the second-order velocity equations (3), while it has been implicitly recognized that the gradient of the continuity equation is zero, the continuity equation itself is no longer part of the system. Mass continuity is thus accounted for only to within an arbitrary constant [22] and

must therefore be explicitly imposed, at least at one point, to remove the arbitrariness of the solution. This can be done by using the continuity equation to modify the original surface integral of the normal velocity equation at exit (Eq. (7)). For example, for an exit normal aligned with the x-axis, the original surface integral

$$\oint_S W_i^Y [(\rho u)_x + 0] \, dy \, dz \qquad (19)$$

is modified, using the continuity equation, to yield

$$-\oint_S W_i^Y [(\rho v)_y + (\rho w)_z] \, dy \, dz. \qquad (20)$$

For the transverse velocity equations, the exit boundary condition is that the normal derivative vanishes. This is accounted for by dropping the first term in the surface integral of the transverse velocity equations. There will, however, be a remaining term that must be evaluated at exit.

The vorticity boundary condition is applied by dropping the first term of the surface integral of Eq. (8), since on the exit boundary the normal derivative of the vorticity is assumed to be zero:

$$(\mu \Omega)_n = 0. \qquad (21)$$

The remaining viscosity source terms in the surface integrals are neglected at the exit.

Wall Boundary Conditions

On walls, no-slip and no-penetration are implemented as Dirichlet conditions on the velocity components:

$$u = 0 \quad \text{or} \quad u = u(S) \qquad (22)$$

$$v = 0 \quad \text{or} \quad v = v(S) \qquad (23)$$

$$w = 0 \quad \text{or} \quad w = w(S). \qquad (24)$$

The vorticity has no explicit wall boundary condition and its definition is used in the following manner at walls:

$$\int_V N_i^\Omega [\Omega - \nabla \times V] \, dV = 0. \qquad (25)$$

IV. SOLUTION PROCEDURE

Stokes flow (Re = 0) is used as an initial guess for flows at all Reynolds numbers. All velocities and vorticities are solved simultaneously. For high Reynolds numbers the solution may require marching through increasingly higher Reynolds numbers. To complete the iteration, for subsonic

flow, the density needs to be updated and this requires the solution for the pressure. This is obtained from a Poisson equation derived by taking the divergence of the momentum equations,

$$\nabla \cdot (\nabla p + F) = 0, \qquad (26)$$

where F is the remainder of the momentum Eqs. (2).

The weighted residual form of the pressure equation is

$$\int_V W_i [\nabla \cdot (\nabla p + F)] \, dV = 0. \qquad (27)$$

Upon integration by parts, one obtains

$$\int_V [\nabla W_i \cdot (\nabla p + F)] \, dV = \int_S [W_i (\nabla p + F) \cdot n] \, dS. \qquad (28)$$

It is seen that the surface integral contains the normal momentum equation. Hence, by neglecting this surface integral on boundaries where the pressure is unknown, the normal momentum equation is automatically satisfied. Such natural boundary conditions of finite element methods are an advantage over schemes where unknowns at a wall may have to be extrapolated from their values in the field. To avoid the arbitrariness of the pressure Poisson problem, the pressure level is set by specifying its value at one point of the flow.

The temperature is updated using the energy equation, once the pressure has been determined. For most of the test cases, the assumption of constant total enthalpy along streamlines was used:

$$H_o = C_p T + \tfrac{1}{2} V \cdot V. \qquad (29)$$

This simplified energy equation is a reasonable approximation for the viscous energy equation in the absence of heat exchange.

The complete energy equation is solved for in a few test cases, in the form

$$\text{Re}(\rho V \cdot \nabla)(C_v T) - \frac{1}{\text{Pr}} \nabla \cdot (k \nabla T) = \Phi - \text{Re}(p \nabla \cdot V). \qquad (30)$$

The weighted residual form of the energy equation, after integration by parts, is

$$\int_V [W_i \, \text{Re}(\rho V \cdot \nabla)(C_v T) + \frac{1}{\text{Pr}} \nabla W_i \cdot (k \nabla T)] \, dV$$

$$= \int_V [W_i (\Phi - \text{Re}(p \nabla \cdot V))] \, dV$$

$$+ \oint_S W_i \frac{1}{\text{Pr}} [n \cdot k \nabla T] \, dS. \qquad (31)$$

The boundary conditions are that either the temperature or the heat flux is specified. The surface integral contains the heat flux allowing a natural implementation of the latter boundary condition.

The density is evaluated from the pressure and temperature, using the equation of state for a perfect gas. The viscosity is finally obtained, using the empirical Sutherland's law for air [28]:

$$\frac{\mu}{\mu_\infty} = \left(\frac{T}{T_\infty}\right)^{1.5}\left(\frac{T_\infty + 110° \text{ K}}{T + 110° \text{ K}}\right). \tag{32}$$

The conductivity and specific heat coefficients are assumed constant.

V. RESULTS

In the present paper, results for laminar incompressible two-dimensional flow are first presented to serve as a comparison against other well-tested numerical methods. The case investigated is the flow in a driven cavity at Re = 100 and 400. The same case is then analyzed in three dimensions, at Reynolds number 100 for both incompressible and compressible flows and at Reynolds number 400 for incompressible flows, and then compared to the results of other numerical methods.

For the two-dimensional case, Fig. 1 shows that convergence to an L_2 residual of 10^{-8} is attained in 11
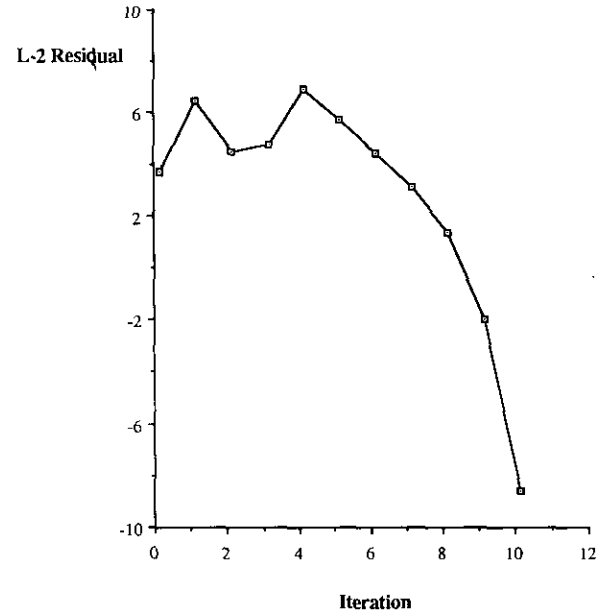
FIG. 1. Convergence history for 2D driven cavity, Re = 400.

iterations on a (15 * 15) element grid. The initial guess needs about five iterations to adjust, due to the corner separation zones, before quadratic convergence is established. Figures 2 and 3 compare equi-vorticity contours and centerline velocities of the present solution to results using the stream function–vorticity method [4].
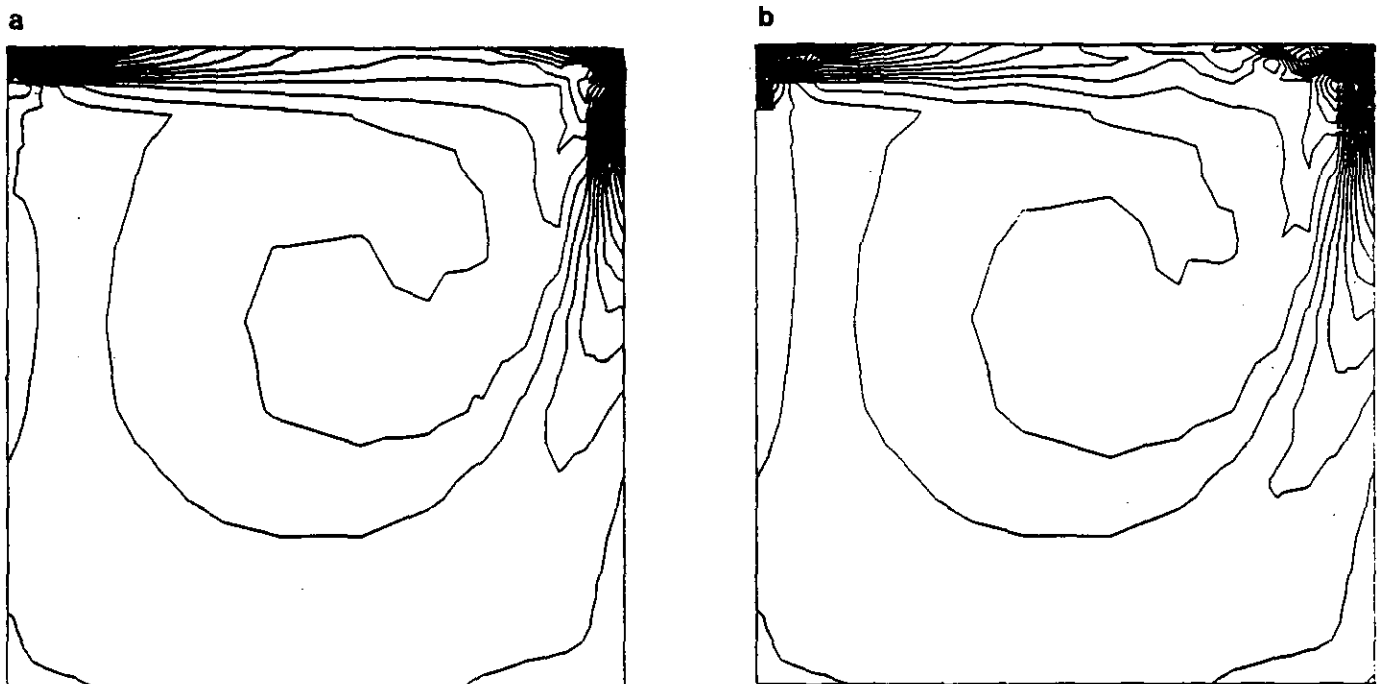

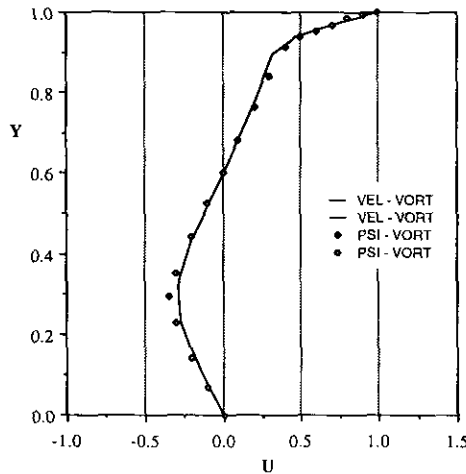FIG. 2. Equi-vorticity lines for 2D driven cavity, Re = 400. a. velocity–vorticity, b. stream function–vorticity.

FIG. 3. Centerline velocities for 2D driven cavity, Re = 400.

The three-dimensional driven cavity problem is analyzed at a Reynolds number of 100. This is carried out for incompressible flow and for lid Mach numbers of 0.2, 0.5, and 0.8. This problem is also analyzed at a Reynolds number of 400 for incompressible flow.

For both the incompressible and subsonic cases, the initial iteration is for incompressible Stokes flow, while subsequent iterations are at the target Reynolds number. Figure 4 compares the convergence history for the incompressible and compressible cases. For incompressible flow, quadratic convergence is attained and machine accuracy
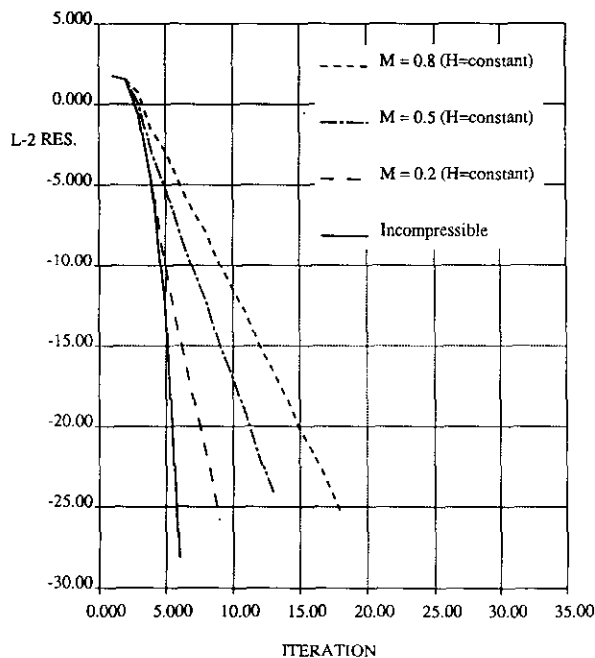
is reached in six iterations. For compressible flow, the pressure, density, temperature, and viscosity are updated in a lagged manner from the velocity–vorticity system, and linear convergence ensues. It must be remarked, however, that the convergence history is still impressive.

In Figure 5, the convergence history is compared for two grids, with the finer one containing eight times the number of elements of the coarse grid. The convergence rate is weakly affected by grid refinement, requiring three additional iterations to reach machine accuracy.

Figure 6 shows the cavity centerline velocities on the symmetric plane for the two- and three-dimensional incompressible cases and compares the 3D results to Ku, Hirsh, and Taylor [29]. Figure 7 shows the effect of compressibility on the cavity centerline velocities on the symmetric plane. Figure 8 shows the normal vorticity contours for the three mid-planes in the incompressible three-dimensional case. These compare very well with the results presented by Osswald, Ghia, and Ghia [21].

For the compressible three-dimensional case, the velocity vectors are shown in Fig. 9 and the density contours in Fig. 10. The trends in the velocity vectors are similar to those presented for incompressible flows.

The compressible three-dimensional cases were redone using the full energy equation instead of the constant total enthalpy assumption. A constant temperature is specified on the moving lid and zero heat flux is imposed on the stationary walls. The convergence history is shown in Fig. 11. Compared to the constant total enthalpy cases (see Fig. 4), convergence is slower and less affected by compressibility.
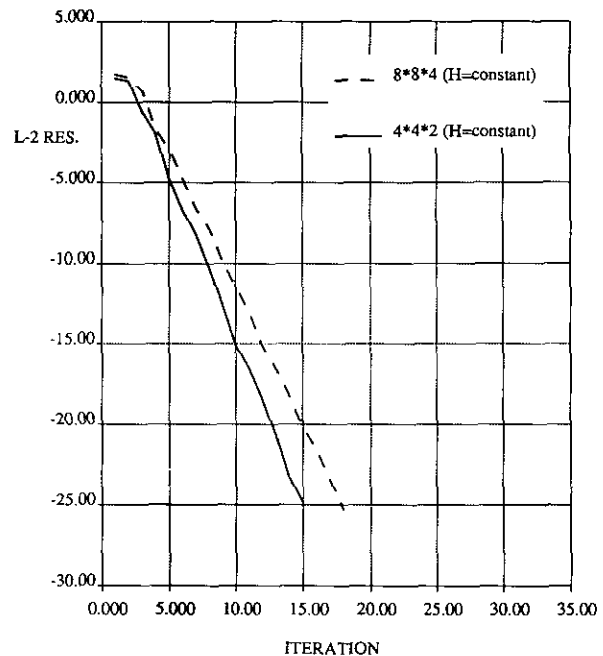

FIG. 4. Convergence history for 3D driven cavity, Re = 100.

FIG. 5. Convergence history for 3D driven cavity, effect of grid size, Re = 100, $M = 0.8$.

FIG. 6. Centerline velocities for 3D driven cavity, Re = 100.
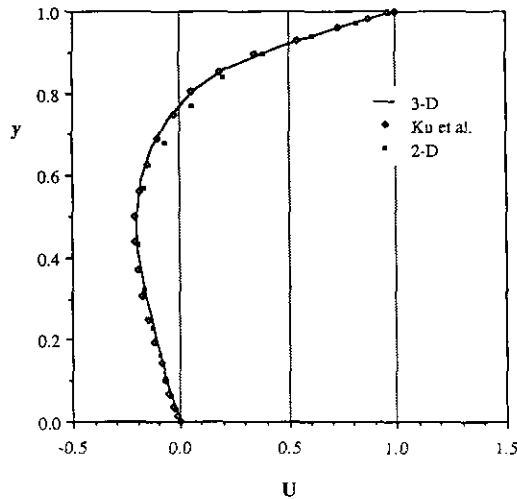
FIG. 7. Centerline velocities for 3D driven cavity, effect of compressibility, Re = 100.

Figure 12 shows the effect of compressibility on the cavity centerline velocities on the symmetric plane. The trends in the centerline velocities are similar to those for the constant total enthalpy cases (see Fig. 7). Temperature contours in the symmetric plane are compared to those of the constant total enthalpy cases in Fig. 13.

For the three-dimensional driven cavity problem for incompressible flow at a Reynolds number of 400, a finer grid is required. Due to the memory requirements of the direct solver for these fine grids, an iterative solver was used. The iterative solver is based on Arnoldi's method, which is a Krylov subspace method for large non-symmetric linear algebraic systems of equations [30]. It is related to the GMRES method and uses the Gram–Schmidt procedure, rather than the modified Gram–Schmidt procedure, to construct the required orthonormal basis of the Krylov subspace, relying on two applications of reorthogonalization [31] to ensure the accuracy and stability of the orthogonalization process.
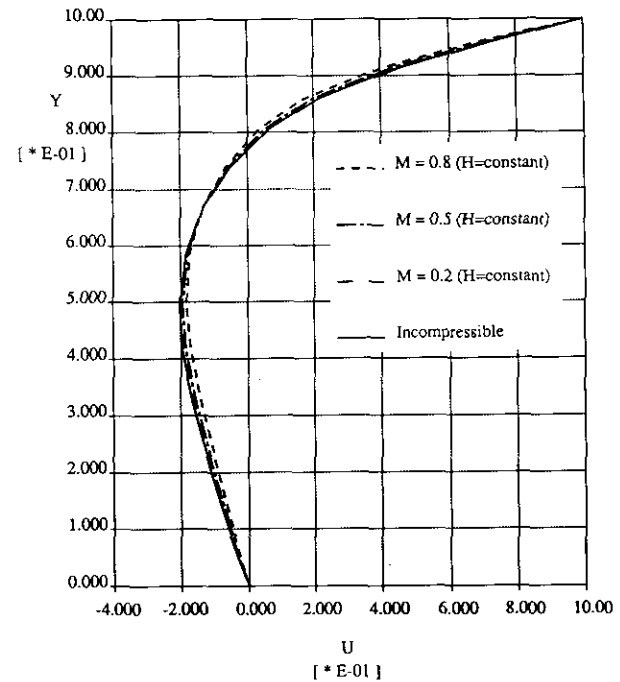
Three grids were used, the two coarser grids solved using the direct solver and the finer grid using the iterative solver. The convergence history for all three grids is shown in Fig. 14. Since the iterative solver is not made to converge completely at each Newton iteration, the overall stability of the method changes. For this particular case, marching in Reynolds number was required. Intermediate solutions at Reynolds numbers of 100 and 200 were obtained before starting at the final Reynolds number of 400. Figure 15 shows the cavity centerline velocities on the symmetric plane for the two- and three-dimensional cases and compares the 3D results to Ku, Hirsh, and Taylor [29] and Agarwal [20]. Figure 16 shows the normal vorticity contours for the three mid-planes.

TABLE I

Maximum Absolute Mass Error

| Re	M	Grid	Energy	Max mass error	Location
100	Incomp.	8 * 8 * 4		0.274E-03	0.96, 0.86, 0.42
100	0.2	8 * 8 * 4	H = const	0.296E-03	0.96, 0.86, 0.42
100	0.5	8 * 8 * 4	H = const	0.408E-03	0.96, 0.86, 0.42
100	0.8	8 * 8 * 4	H = const	0.594E-03	0.96, 0.86, 0.42
100	0.2	8 * 8 * 4	Energy equation	0.283E-03	0.96, 0.86, 0.42
100	0.5	8 * 8 * 4	Energy equation	0.392E-03	0.96, 0.86, 0.42
100	0.8	8 * 8 * 4	Energy equation	0.576E-03	0.96, 0.86, 0.42
400	Incomp.	8 * 8 * 4		0.288E-03	0.96, 0.86, 0.42
400	Incomp.	14 * 14 * 7		0.962E-04	0.03, 0.97, 0.03
400	Incomp.	30 * 30 * 15		0.144E-04	0.01, 0.99, 0.48
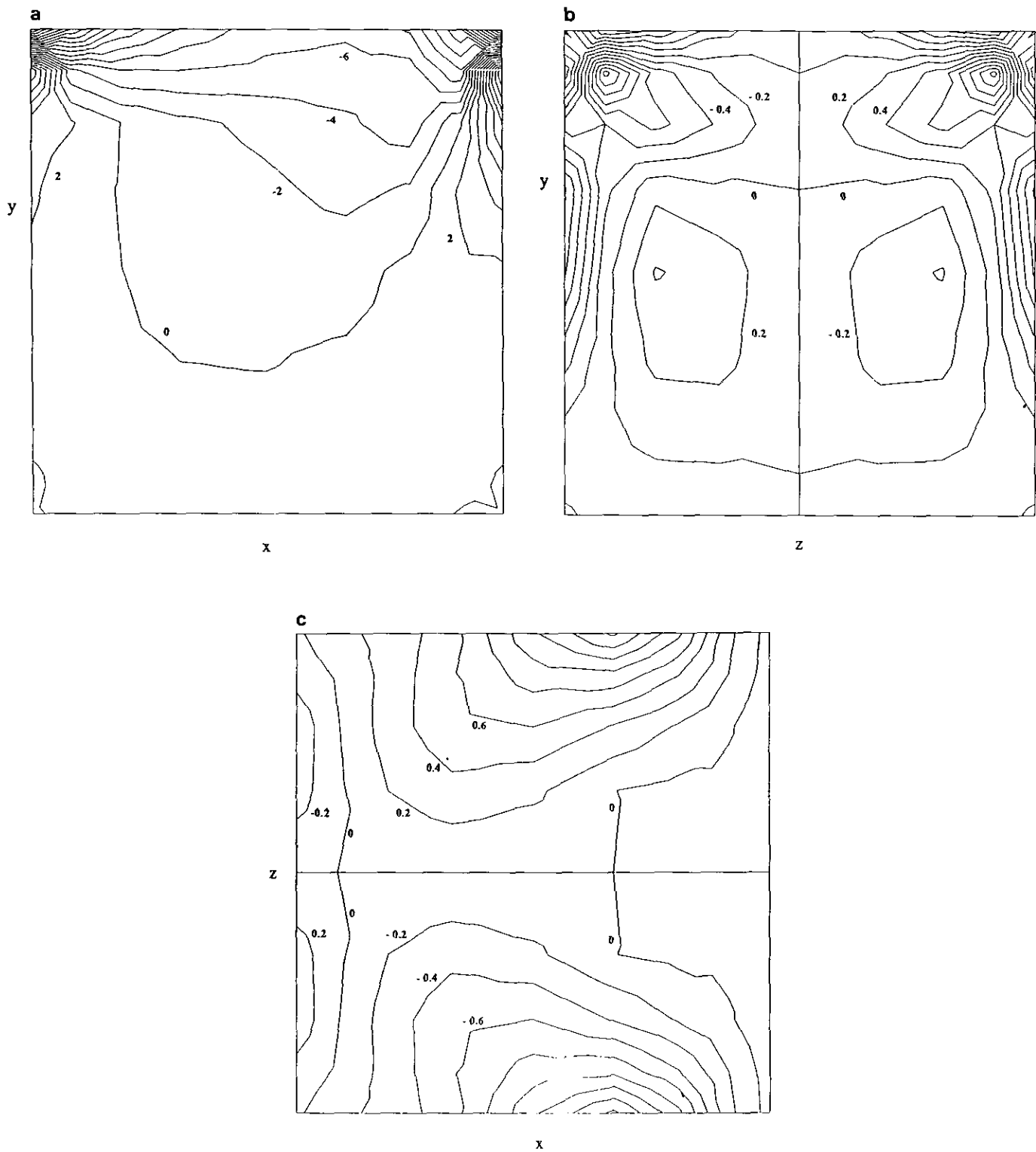
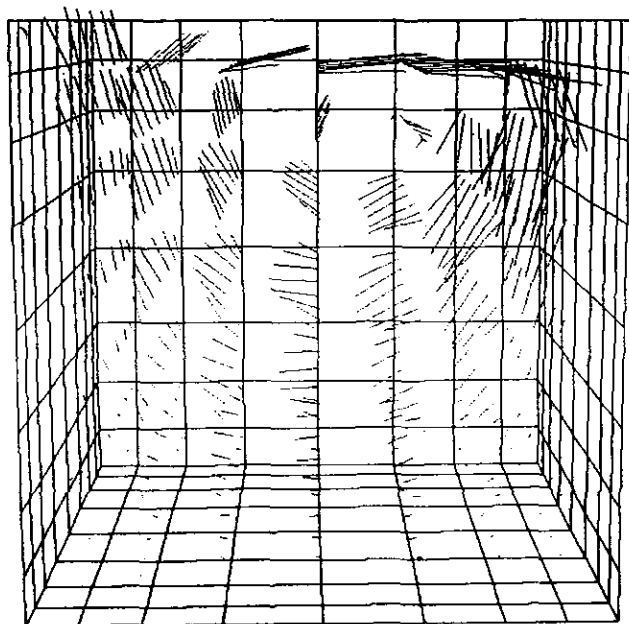**FIG. 8.** 3D driven cavity, Re = 100, mid-plane-normal vorticity lines. a. streamwise, b. spanwise, c. horizontal.

FIG. 9. Velocity vectors for 3D driven cavity, Re = 100, M = 0.5.

The continuity equation is not solved for explicitly, as shown in Section III. To assess the error in mass conservation for each element in the domain the following measure was evaluated:

$$E^e_{mass} = \int_{S^e} (\mathbf{V} \cdot \mathbf{n}) \, dS.$$

The maximum absolute error from all the elements is tabulated for each test case in Table I. The trends show that the mass conservation error increases with Mach number,

CONTOUR
LEVELS
1.00000
1.02500
1.05000
1.07500
1.10000
1.12500
1.15000
1.17500
1.20000
1.22500
1.25000
1.27500
1.30000
1.32500
1.35000
1.37500
1.40000
1.42500
1.45000
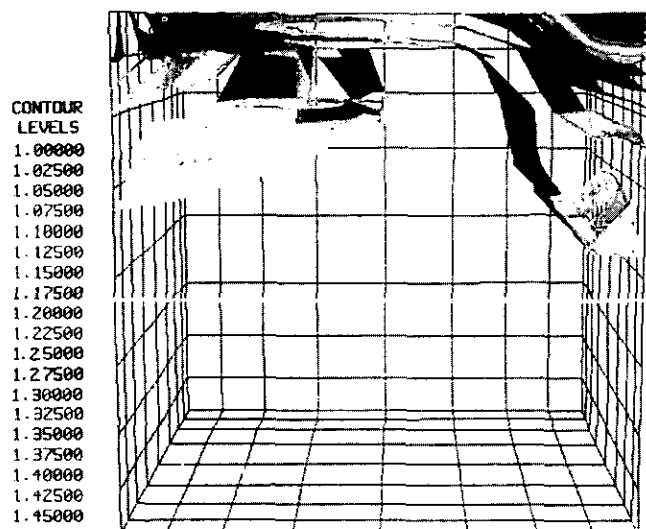
FIG. 10. Density contours for 3D driven cavity, Re = 100, M = 0.5.
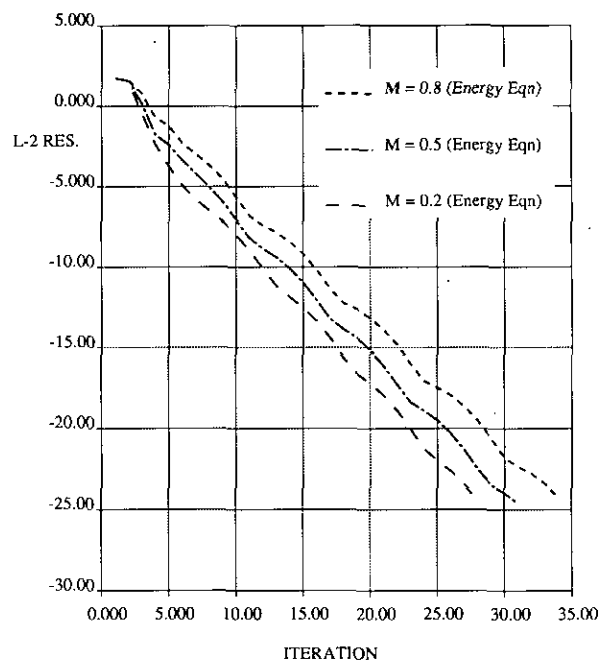
FIG. 11. Convergence history for 3D driven cavity, energy equation, Re = 100.

increases slightly with Reynolds number, decreases with grid size, and is slightly lower for the full energy equation than for the constant total enthalpy assumption.
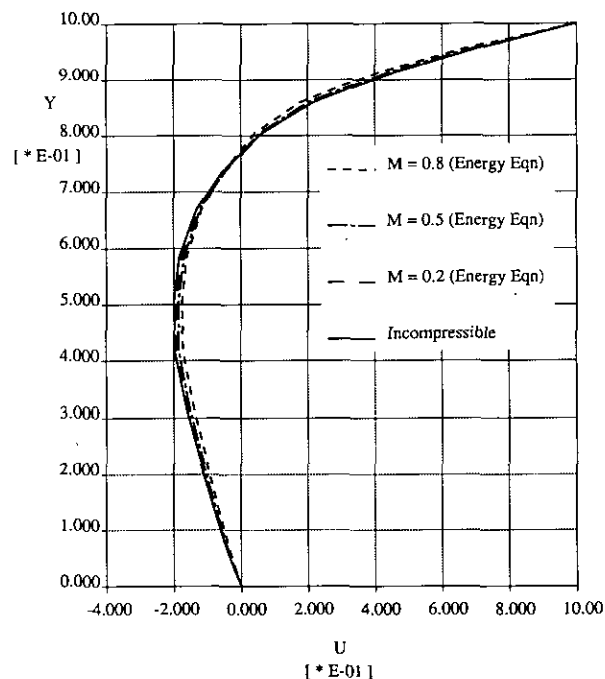

FIG. 12. Centerline velocities for 3D driven cavity, effect of compressibility, energy equation, Re = 100.
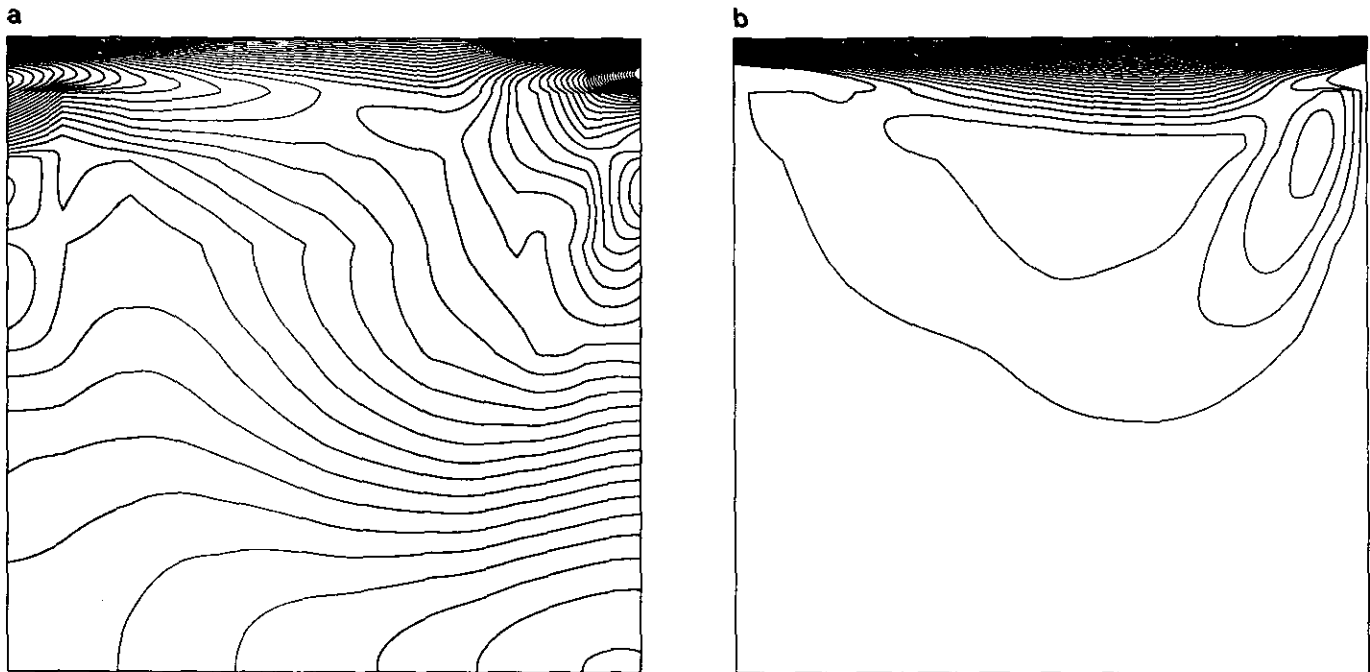
FIG. 13. 3D driven cavity, Re = 100, constant temperature lines, symmetric plane. a. energy equation, b. constant total enthalpy.
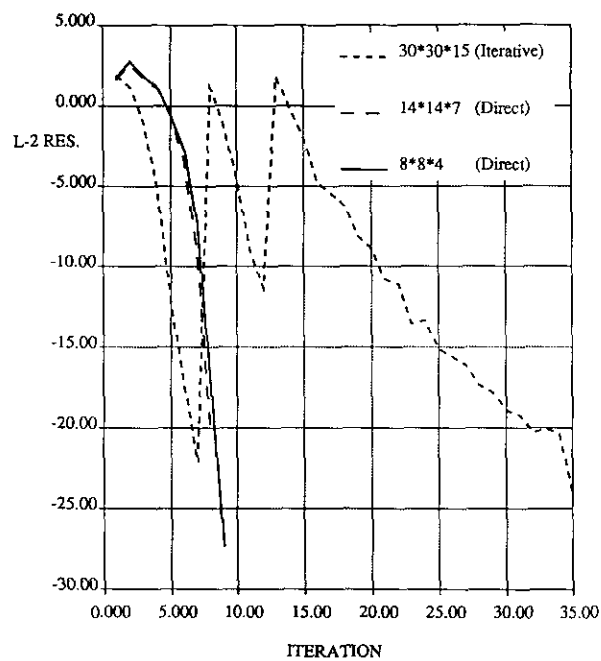

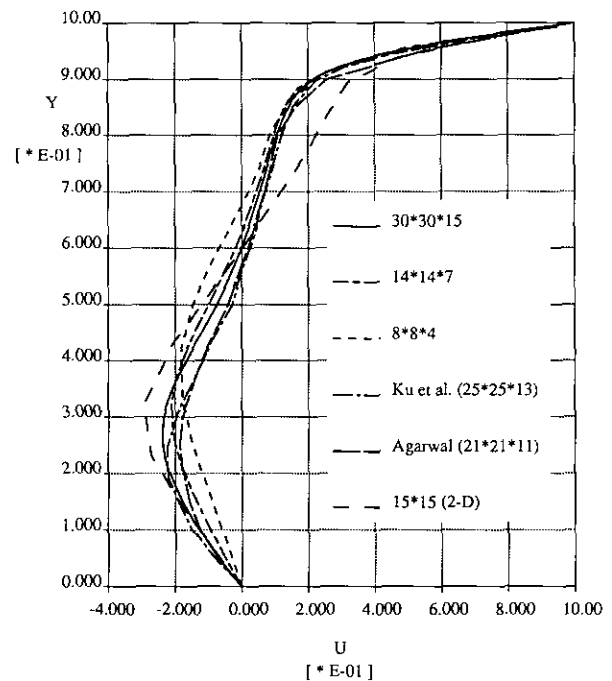**FIG. 14.** Convergence history for 3D driven cavity, Re = 400.

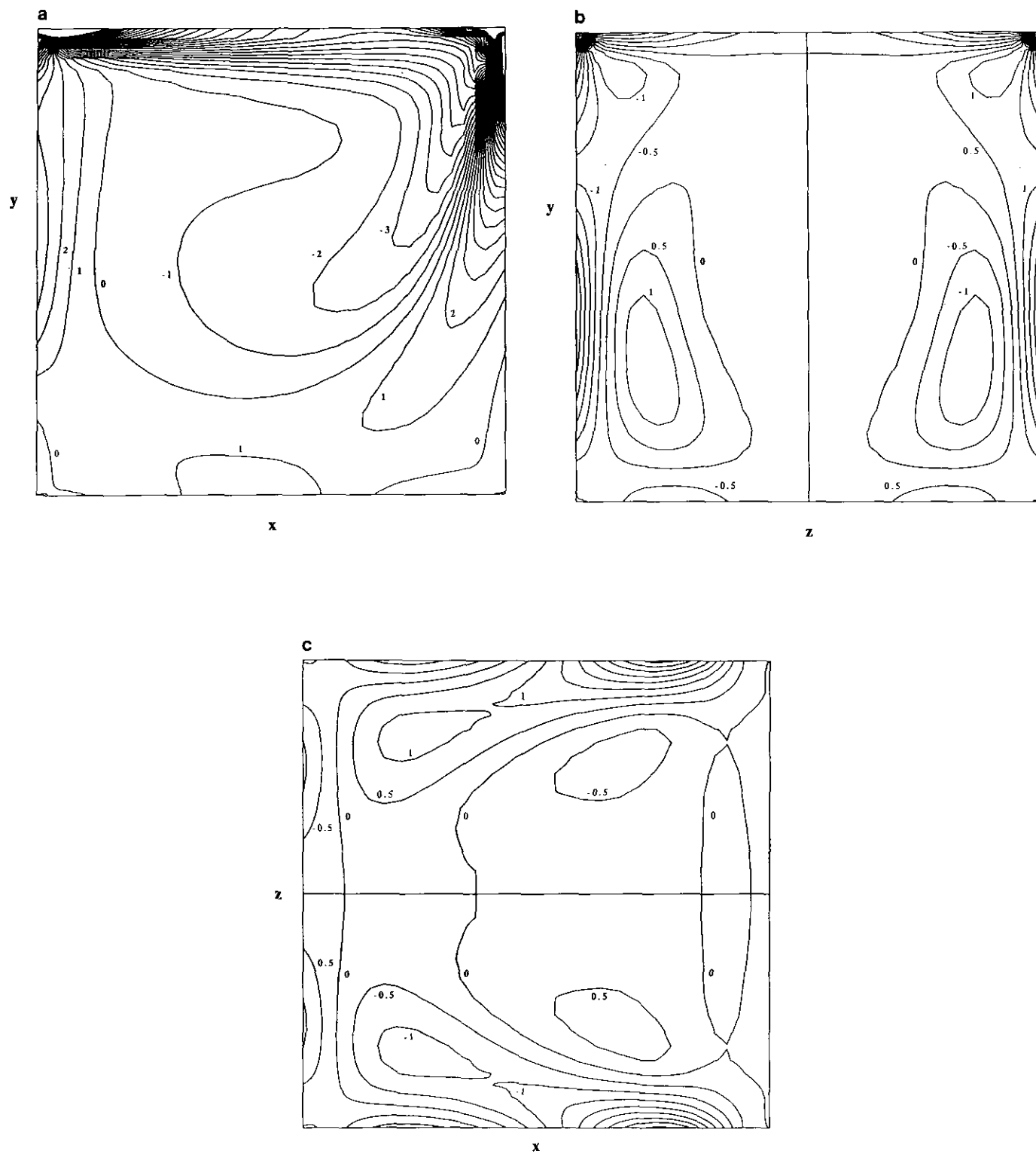**FIG. 15.** Centerline velocities for 3D driven cavity, Re = 400.

FIG. 16.   3D driven cavity, Re = 400, mid-plane-normal vorticity lines. a. streamwise, b. spanwise, c. horizontal.

VI. CONCLUSION

In conclusion, finite element solutions of the three-dimensional Navier–Stokes equations in velocity–vorticity form have been obtained for laminar compressible flow. Solving the velocity–vorticity system simultaneously by a Newton method leads to a fast convergence rate for the test cases shown.

Current work concerns extending the methodology to turbulent high Reynolds number flows. For the large velocity–vorticity system required, iterative solvers and domain decomposition methods, on parallel computers, are being studied.

ACKNOWLEDGMENTS

REFERENCES

1. A. Campion-Renson and M. J. Crochet, *Int. J. Numer. Methods Eng.* 12, 1809 (1978).

2. G. Dhatt, B. K. Fomo, and C. A. Bourque, *Int. J. Numer. Methods Eng.* 17, 199 (1981).

3. W. N. R. Stevens, *Int. J. Numer. Methods Fluids* 2, 349 (1982).

4. M. F. Peeters, W. G. Habashi, and E. G. Dueck, *Int. J. Numer. Methods Fluids* 7, 17 (1987).

5. A. Mizukami, *Int. J. Numer. Methods Eng.* 19, 1403 (1983).

6. W. G. Habashi, M. F. Peeters, G. Guevremont, and M. M. Hafez, *AIAA J.* 25, 944 (1987).

7. M. M. Hafez, W. G. Habashi, S. M. Przybytkowski, and M. F. Peeters, AIAA Paper 87-0944, Reno, Nevada, 1987 (unpublished).

8. T. E. Tezduyar, R. Glowinski, and F. Glaisner, in *Numerical Methods in Laminar and Turbulent Flow*, edited by C. Taylor, W. G. Habashi, and M. M. Hafez (Pineridge Press, Swansea, UK, 1987), p. 197.

9. G. J. Hirasaki and J. D. Hellums, *Q. Appl. Math.* 26, 331 (1968).

10. G. J. Hirasaki and J. D. Hellums, *Q. Appl. Math.* 28, 293 (1970).

11. H. Yang and R. Camarero, *Int. J. Numer. Methods Fluids* 6, 35 (1986).

12. A. Sherif and M. M. Hafez, AIAA Paper 83-1948-CP, 1983 (unpublished).

13. R. L. Davis, J. E. Carter, and M. M. Hafez, AIAA Paper 87-0601, Reno, Nevada, 1987 (unpublished).

14. A. Hamed and S. Abdallah, *J. Fluids Eng. Trans. ASME* 108, 348 (1986).

15. F. El Dabaghi, AIAA Paper 85-1532-CP, Cincinnati, Ohio, 1985 (unpublished).

16. F. El Dabaghi and O. Pironneau, *Numer. Math.* 48, 561 (1986).

17. H. Fasel, *J. Fluid Mech.* 78, 355 (1976).

18. R. N. Cook, Ph.D. Thesis, University of Western Ontario, 1976 (unpublished).

19. S. C. R. Dennis, D. B. Ingham, and R. N. Cook, *J. Comput. Phys.* 33, 325 (1979).

20. R. K. Agarwal, in *Computers in Flow Predictions and Fluid Dynamics Experiments*, edited by K. N. Ghia, T. J. Mueller, and B. R. Patel (ASME, New York, 1981), p. 73.

21. G. A. Osswald, K. N. Ghia, and U. Ghia, in *Proceedings AIAA 8th Computational Fluid Dynamics Conference*, Honolulu (AIAA, Washington, DC, 1987), p. 408.

22. A. Toumi and T. Phuoc Loc, in *Numerical Methods in Laminar and Turbulent Flow*, edited by C. Taylor, W. G. Habashi and M. M. Hafez (Pineridge Press, Swansea, UK, 1987), p. 595.

23. R. A. Nicolaides, in *Finite Element Analysis in Fluids*, edited by T. J. Chung and G. R. Karr (UAH Press, Huntsville, AL, 1989), p. 824.

24. M. D. Gunzburger, M. Mundt, and J. S. Peterson, in *Computational Methods in Viscous Aerodynamics*, edited by C. A. Brebbia (Springer-Verlag, New York, 1990).

25. T. Gatski, C. E. Grosch, and M. E. Rose, *J. Comput. Phys.* 82, 298 (1989).

26. G. Guevremont, W. G. Habashi, M. M. Hafez, and M. F. Peeters, in *Proceedings, 4th International Conference on Computational Engineering Science, Atlanta*, edited by S. N. Atluri and G. Yagawa (Springer-Verlag, New York, 1988), p. 51.x.1.

27. W. G. Habashi, G. Guevremont, M. F. Peeters, S. M. Przybytkowski, and M. M. Hafez, in *Computational Methods in Viscous Aerodynamics*, edited by C. A. Brebbia (Springer-Verlag, New York, 1990).

28. H. Schlichting, *Boundary Layer Theory*, 7th ed. (McGraw-Hill, New York, 1979), p. 328.

29. H. C. Ku, R. S. Hirsh, and T. D. Taylor, *J. Comput. Phys.* 70, 439 (1987).

30. Y. Saad and M. H. Schultz, *SIAM J. Sci. Stat. Comput.* 7, 856 (1986).

31. J. H. Wilkinson, *The Algebraic Eigenvalue Problem* (Oxford Univ. Press, London, 1965), p. 328.